Polarization-maintaining photonic crystal fiber with rim-touched defect-holes

Jui-Ming Hsu [a,b,*], Cheng-Ling Lee [a,b], Jing-Shyang Horng [a,b], Jerry Ji-Ho Kung [a,b]

[a] Department of Electro-Optical Engineering, National United University, Miaoli, Taiwan 360, R. O. C.
[b] Optoelectronics Research Center, National United University, Miaoli, Taiwan 360, R. O. C.

ARTICLE INFO

ABSTRACT

To achieve a polarization-maintaining photonic crystal fiber (PM-PCF) with ultra-high modal birefringence, four types of PM-PCF structure, Traditional, Rim-Touched -4 and -5 (RTS-4 and RTS-5) and Air-Walls structures (AWS), are investigated and compared with each other. A compromising structure with higher birefringence, lower loss and feasibility can be chosen by means of numerical analysis. From the simulation results, the birefringence of the designed RTS-4 PM-PCF with a confinement loss of only about 0.395 dB/km is up to 13.22×10^{-3} at $\lambda = 1.55 \ \mu m$. Finally, two imperfect conditions of broken wall and thicker wall in the drawing process are investigated to prove that the proposed structure is practicable.

1. Introduction

In conventional single mode fibers (SMF), unpredictable birefringence brings about polarization-mode dispersion (PMD) and induces pulse broadening; results in serious restrictions in the data rates of high-speed optical communication links. Conventional polarization-maintaining fibers (PMF, such as elliptical core fibers, bowtie structured fibers, and PANDA fibers) with a modal birefringence about 10^{-4} order typically, which are designed to significantly reduce the governing factor of small random birefringence fluctuations.

Recently many articles used photonic crystal fibers (PCF) to realize a polarization-maintaining photonic crystal fiber (PM-PCF) [1–7]. Modal birefringence of about 10^{-3} order is achieved typically for PM-PCF at a wavelength of 1.55 μm. T. P. Hansen et al. designed two neighboring solid rods to consist an asymmetric elliptical core [3]. T. Nasilowski et al. used three solid rods instead of using two rods to form a highly elliptical core [5]. M. Chen et al. used three solid rods and four big elliptical air-holes to replace the holes nearest the central rod [6].

In this study, four types of PM-PCF indicated in Fig. 1 are simulated and compared with each other. Traditional type

(Fig. 1(a)) with three solid rods is similar to the structures proposed in [5,6]; nevertheless, four pairs of larger holes, which are named as defect-holes in this article, are used near the elliptical core instead of cladding holes. Rim-Touched Structure (RTS) with defect-holes touch rim by rim with each other inseparably. Two types of RTS PM-PCF are simulated in this article; RTS-5 and RTS-4 with five and four pair of rim-touched defect-holes are shown as Fig. 1(b) and (c), respectively. Air-Walls Structure (AWS, Fig. 1(d)) with two strip of air, which is designated as "air walls" in this article, near the elliptical core achieves maximum birefringence in the four types of PM-PCF; however it is difficult to be realized. Finally, a compromising approach is selected and designed with some tradeoff between fabrication-difficulty, birefringence and confinement loss.

2. Simulation models

The cross-sectional views of four types of PM-PCF structure are shown in Fig. 1(a)–(d), respectively. In Fig. 1(a), Traditional structure consists of a triangular lattice of cladding holes with a diameter of $d_S = 1.00 \ \mu m$, and a pitch of $\Lambda = 1.68 \ \mu m$. The eight defect-holes (colored in yellow) with a diameter of d_L situated at both sides of the elliptical core. Fig. 1(b) shows the RTS-5 structure with the same geometric parameters Λ, d_S and d_L with the Traditional one in Fig. 1(a). Five defect-holes (colored in yellow) at each side of the elliptical core touch rim by rim with each other inseparably. For the sake of comparison, the diameters

* Corresponding author at: National United University, Department of Electro-Optical Engineering, No.1, Lienda Rd., Kung-Ching Li, Miaoli 360, Taiwan, ROC. Tel.: +886 37 38 1725; fax: +886 37 35 1575.
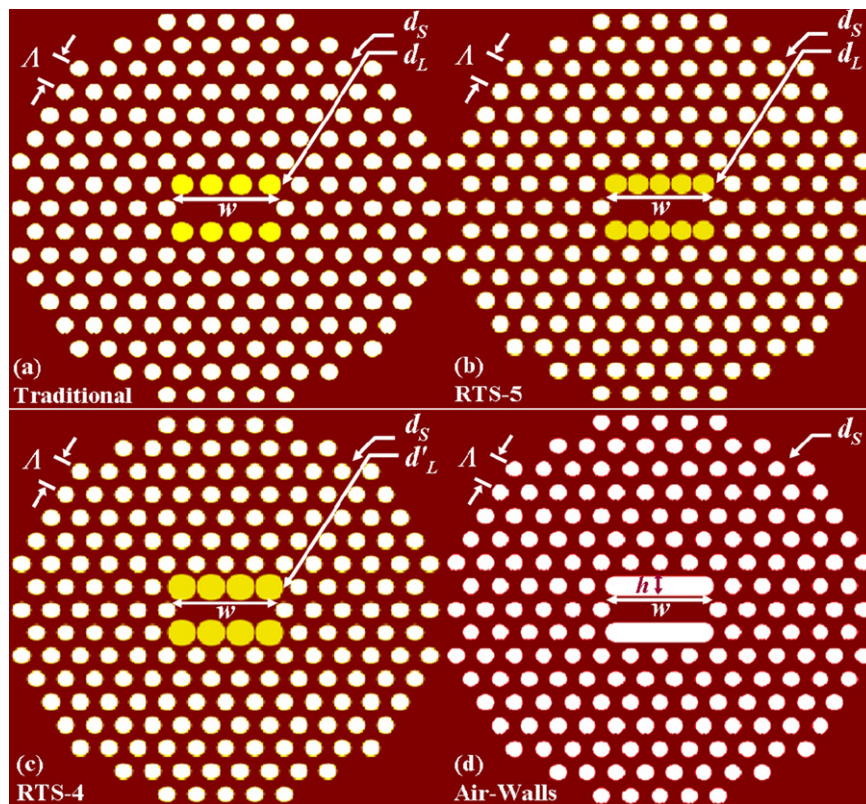E-mail addresses: jmhsu@nuu.edu.tw, juiminghsu@gmail.com (J.-M. Hsu).

Fig. 1. Cross-sectional views of (a) Traditional structure, (b) RTS-5, (c) RTS-4 and (d) Air-Walls structure PM-PCFs. $\Lambda = 1.68$ μm, $d_S = 1.00$ μm, $d_L = h = 1.26$ μm, $d'_L = 1.68$ μm. (For interpretation of the references to color in this figure legend, the reader is referred to the web version of this article.)

d_S and d_L are designed to be identical between the Traditional and RTS-5 structures. Therefore, $w = 3\Lambda + d_L$ in Fig. 1(a) must be equal to $w = 5d_L$ in Fig. 1(b); as a result, the size of the defect-holes $d_L = 3\Lambda/4 = 1.26$ μm is evaluated for these two types of PM-PCF. Fig. 1(c) shows the RTS-4 structure with only four pair of defect-holes. To touch the defect-holes rim by rim with each other, the size of the defect-holes $d'_L = \Lambda = 1.68$ μm is selected for the RTS-4 PM-PCF. Fig. 1(d) exhibits the AWS structure. For the sake of comparison again, two air-walls with a height of $h = d_L = 1.26$ μm and a width of $w = 3\Lambda + d_L = 6.3$ μm are used in place of four and five large holes in the Traditional and RTS-5 structures.

3. Numerical results and discussions

The modal birefringence of a fiber is defined as the difference in effective refractive index of the slow mode and fast mode

$$B = |n_{slow} - n_{fast}|, \tag{1}$$

where B is the modal birefringence of a fiber, n_{slow} and n_{fast} represent the effective refractive index of the slow and fast modes propagated in the fiber. In this study, n_{slow} and n_{fast} can be evaluated by means of the plane-wave expansion (PWE) method for each type of structures; the B values at a range of wavelength are then figured out by using Eq. (1).

Fig. 2 shows the dependence of birefringence on wavelength for four types of PM-PCFs indicated in Fig. 1. As shown in Fig. 2, the birefringence value of AWS structure is largest among the four types of PM-PCF. However, for accomplishing the air-walls in the fiber is quite difficult. The modal birefringence of RTS structures (RTS-4 and RTS-5) are just less than that of AWS structure slightly and greatly larger than that of Traditional structure. Nevertheless, its fabrication process is considerably simpler than that of AWS
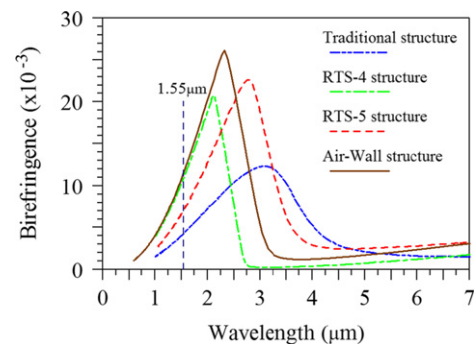

Fig. 2. Dependence of birefringence on wavelength for 4 types of PM-PCFs shown in Fig. 1.

structure. Therefore, Traditional and AWS structure are eliminated from the consideration of the design in this work. For the two RTS structures, the peak value of the birefringence curve of the RTS-5 is larger than that of the RTS-4. However, at the habitual wavelength of optical-fiber communications (1.55 μm), the birefringence of the RTS-4 is larger than that of the RTS-5. Therefore, it is worthy for comparing RTS-4 with RTS-5 in detail by the birefringence and confinement loss.

Fig. 2 reveals that the maximum values of birefringence for the two types of RTS structures are occurred at a wavelength which is too far from a wavelength of 1.55 μm. To shift the maximum-birefringence wavelength toward a wavelength of 1.55 μm while still keeping its birefringence at an original value, the whole structure can be shrunken with a scale-down factor α [7]. For the sake of convenience, the α is defined as a shrink ratio of geometric parameter. The structure will be scaled down with the hole-diameters (d_S, d_L and d'_L) and pitch (Λ) in a same ratio α.

Fig. 3(a) and (b) respectively indicate the relationship between the birefringence and wavelength for the considered RTS-5 and RTS-4 structures with various shrink ratio α. For the case of $\alpha=1$, the structures represent the unshrinking PM-PCFs. Therefore, the curves of birefringence for $\alpha=1$ shown in Fig. 3(a) and (b) are identical to that of RTS-5 and RTS-4 structures shown in Fig. 2. As shown in Fig. 3(a) and (b), the maximum values of birefringence for each shrunken structure are almost identical. However, the wavelength that a maximum birefringence occurred is shifted to a shorter wavelength when α is decreased. As shown in the figures, $\alpha=0.565$ for RTS-5 and $\alpha=0.735$ for RTS-4 achieve a maximum birefringence at a wavelength of around 1.55 μm.

To design a structure trading higher birefringence for an acceptable loss, this work proceeds to study the confinement loss for the two types of RTS structures with various α. The confinement loss (L_C) for each case is deduced by the value of the imaginary part of effective indices (n_{eff}) as

$$L_C = 8.686 \times k_o \times Im[n_{eff}], \tag{2}$$

in dB/m, where k_o is the wave number in free space, $Im[n_{eff}]$ represents the imaginary part of n_{eff}. The numeric results of the birefringence and the confinement loss (in logarithmic scale) for RTS-4 and RTS-5 structures, at a wavelength of 1.55 μm, as a function of α are shown in Fig. 4. As is obvious from the figure, if the α is set to achieve a maximum birefringence, the PM-PCF is unrealistic owing to an extremely large loss. An upper loss-limit of 0.5 dB/km is set and labeled in Fig. 4. The designed PM-PCF is expected that its confinement loss is suppressed to lower than the upper loss-limit in this work. As shown in the figure, the birefringence of the RTS-4 is larger than that of the RTS-5 in the case of same loss. Therefore, the RTS-4 is selected as the best structure for designing a good performance PM-PCF. To depress the loss under 0.5 dB/km, $\alpha=0.92$ is selected for the compromising PM-PCF structure. The geometric parameters of the designed RTS-4 structure PM-PCF are ultimately designed and recorded as
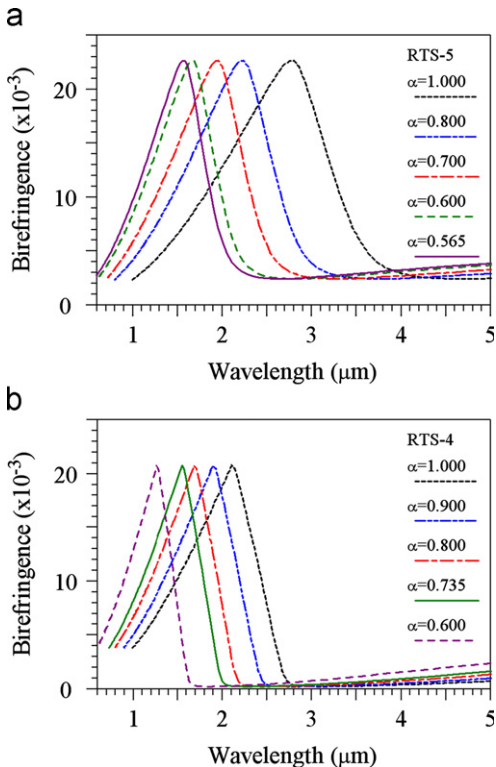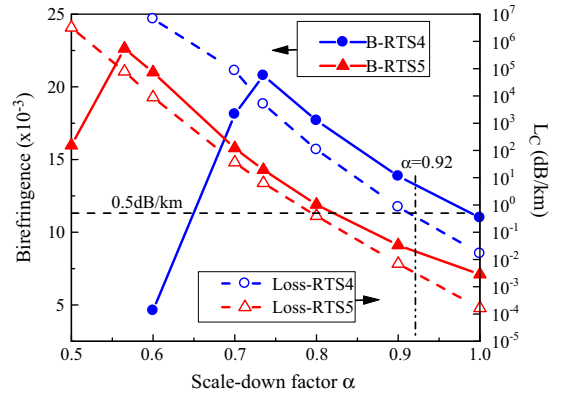

Fig. 4. Birefringence (B) and confinement loss (L_C, in logarithmic scale) for RTS-4 and RTS-5 structures as a function of shrink ratio α at a wavelength of 1.55 μm. $\Lambda = \alpha \times 1.68$ μm, $d_S = \alpha \times 1.00$ μm, $d_L = \alpha \times 1.26$ μm, $d'_L = \alpha \times 1.68$ μm.

follows: the pitch $\Lambda = 1.68 \times 0.92 \approx 1.5456$ μm, the cladding holes diameter $d_S = 1.00 \times 0.92 = 0.9200$ μm, the defect-holes diameter $d'_L = 1.68 \times 0.92 \approx 1.5456$ μm. As shown in Fig. 4, the birefringence value is up to 13.22×10^{-3} at a wavelength of 1.55 μm; moreover, the confinement loss of the structure is about 0.395 dB/km.

4. Fabrication and imperfect models

The manufacturing process of the Rim-Touched PM-PCF is similar to that of an ordinary PCF. The preform of the proposed RTS4 PM-PCF can be fabricated by introducing eight extremely thin capillary silica tubes instead of the ordinary capillary tubes at the defect-holes position during the stacking process. To maintain a perfect appearance of the Rim-Touched structure, even more careful control of the drawing process is necessary. A lower temperature level, a slight overpressure inside the preform, and a proper drawing-speed adjusting are helpful to the drawing process [8]. However, since the walls between the defect-holes are so thin, they maybe break even though the drawing process is carefully controlled. To examine the influence of the broken-wall on the RTS-4 structure, a broken-wall model is built for comparing with a normal model. It is reasonable for setting the size of the defect-holes larger than that of the original slightly in simulation, then the walls between the defect-holes may slightly "break" as shown in Fig. 5(a). The overlap percentage, which is notated as η in this article, is defined as the incremental percentage for the diameter of defect-holes, e.g. $\eta=1\%$ means that the defect-holes with a diameter of 1.01D. Fig. 5(a) and (b) indicates the defect-holes of a broken wall model with an η of 1% and a normal model, respectively. Fig. 5(c) reveals the dependence of birefringence and confinement loss on overlap percentage (η) for RTS-4 structure with a shrink ratio (α) of 0.92 at a wavelength of 1.55 μm. As shown in the figure, the birefringence increases with the η. This can be considered that the larger the η, the composition of defect-holes is more similar with an Air Wall, and then the birefringence is increased (refer to Fig. 2). Furthermore, the confinement losses of the broken wall models shown in Fig. 5(c) are still acceptable. In conclusion, the broken wall imperfect arisen from the drawing process may raise the birefringence of the PM-PCF, while the confinement loss is limited in an acceptable level.

To avoid the imperfect of broken wall, one may increase the thickness of the defect-hole walls in the preform, that is to say, one may decrease the size of the defect-holes. It is worth investigating the properties of the RTS-4 PM-PCF during the thickness of the hole-walls changes. Fig. 6 indicates the birefringence and the confinement loss for RTS-4 structure with a shrink
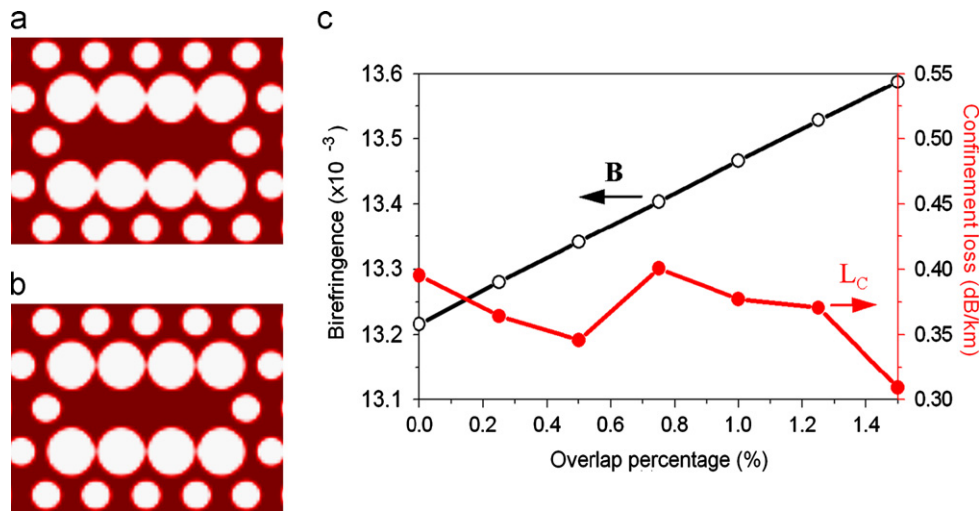

Fig. 3. Relationship between birefringence and wavelength for (a) RTS-5 and (b) RTS-4 with various shrink ratio α.

Fig. 5. Cross-up views of RTS-4 structures of (a) broken-wall model (with $\eta=1\%$), and (b) normal model. (c) Dependence of birefringence and confinement loss on overlap percentage (η) for RTS-4 structure with a shrink ratio of 0.92 at a wavelength of 1.55 μm. $\Lambda=0.92 \times 1.68$ μm, $d_S=0.92 \times 1.00$ μm, $d'_L=\eta \times 0.92 \times 1.68$ μm.
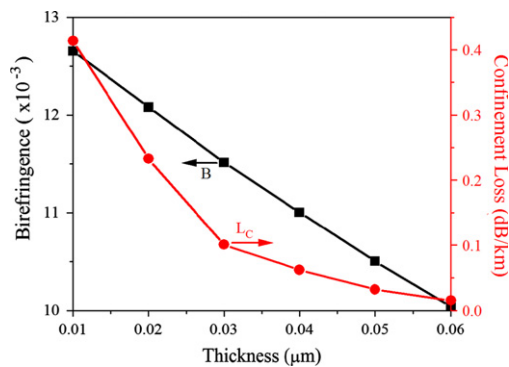

Fig. 6. Birefringence and confinement loss for RTS-4 structure with $\alpha=0.92$ as a function of wall-thickness (t) at a wavelength of 1.55 μm. $\Lambda=0.92 \times 1.68$ μm, $d_S=0.92 \times 1.00$ μm, $d'_L=\Lambda-2t$.

ratio (α) of 0.92 as a function of wall-thickness at a wavelength of 1.55 μm. As shown in the figure, both the birefringence and the confinement loss decrease as the thickness of defect-hole walls increases. In conclusion, for the sake of reserving a tolerance of broken wall imperfect arises from the drawing process, one may decrease the size of defect-holes. Consequently, the birefringence will be decreased. However, the thick walls accompany that drawback with a benefit fortunately, the loss is decreased too.

The investigations of two imperfect conditions of broken wall and thicker wall verify that both the birefringence and the confinement loss are still well-performing while the imperfects are occurred in the drawing process. The numerical results can be used as a reference of design for defect-holes and regarded as a trade-off between the modal birefringence and confinement loss.

5. Conclusions

Four types of elliptical core polarization-maintaining photonic crystal fiber are theoretically investigated and compared with

each other by their modal birefringence values. The Air-Walls structure has a largest birefringence, while it is quite difficult to fabricate. On the contrary, the Traditional structure is easy to realize, but its birefringence is smallest among the four types of structure. As a happy medium, the Rim-Touched structure not only has a large birefringence value close to an Air-Walls structure but it is easy to carry out. To shift the wavelength for maximum birefringence occurred toward the habitual wavelength of optical-fiber communications (1.55 μm), one may shrink the Rim-Touched structures with an appropriate ratio. Comparing the confinement loss between the two Rim-Touched types, the RTS-4 is better than the RTS-5 structures. Ultimately, the birefringence of the designed RTS-4 PM-PCF with a pitch of 1.5456 μm, a cladding-holes diameter of 0.9200 μm, and a large-holes diameter of 1.5456 μm is up to 13.22×10^{-3} at a wavelength of 1.55 μm; moreover, the confinement loss of the structure is only about 0.395 dB/km. Finally, considering a realistic condition, two imperfect conditions of broken wall and thicker wall in the drawing process are investigated. The numerical results verify that both the birefringence and the confinement loss are still well-performing while the imperfects are occurred in the fabrication process.

References

[1] A. Ortigosa-Blanch, J.C. Knight, W.J. Wadsworth, J. Arriaga, B.J. Mangan, T.A. Birks, P.S.J.P.St.J. Russell, Optics Letters 25 (2000) 1325.
[2] K. Suzuki, H. Kubota, S. Kawanishi, M. Tanaka, M. Fujita, Optics Express 9 (2001) 676.
[3] T.P. Hansen, J. Broeng, S.E.B. Libori, E. Knudsen, A. Bjarklev, J.R. Jensen, H.R. Simonsen, IEEE Photonics Technology Letters 13 (2001) 588.
[4] Y.S. Sun, Y.F. Chau, H.H. Yeh, L.F. Shen, T.J. Yang, D.P. Tsai, Applied Optics 46 (2007) 5276.
[5] T. Nasilowski, et al., Applied Physics B 81 (2005) 325.
[6] M. Chen, S.G. Yang, F.F. Yin, H.W. Chen, S.Z. Xie, Opto-Electronics Letters 4 (2008) 19.
[7] J.M. Hsu, G.S. Ye, D.L. Ye, Fiber and Integrated Optics 31 (2012) 11.
[8] F. Poli, A. Cucinotta, S. Selleri, Photonic Crystal Fibers Properties and Applications, Springer, Dordrecht, Netherlands, 2007.